

PRELIMINARY RESULTS OF A COMPACT LINEAR ACCELERATOR FOR AN ION BEAM

RESULTADOS PRELIMINARES DE UN ACELERADOR LINEAL COMPACTO PARA UN HAZ DE IONES

Víctor Alfonso Díaz Gómez¹
 Edwin Munévar Espitia²
 José Alfonso Leyva Rojas³

Abstract

For more than three decades, computational simulations of ion beam extraction have been used in ion acceleration systems. This paper describes a simulation in MATLAB R2020a of a seven-electrode ion extraction system. The purpose of this work is to determine whether certain parameters of the extraction system, such as the plasma meniscus and the beam interface, can be accurately modeled and thus used to successfully predict the ion trajectory and beam shape over a wide range. Various electrode configurations in accelerator columns are analyzed, and one is selected for a more detailed description in this work.

Keywords: Linear accelerators, ion trajectory, extraction systems, acceleration systems, electric fields, equipotential lines, ion implantation, medical imaging, proton therapy.

Resumen

Durante más de tres décadas, las simulaciones computacionales de extracción por haz de iones se han utilizado en sistemas de aceleración de iones. Este artículo describe una simulación en MATLAB R2020a de un sistema de extracción de iones de siete electrodos. El propósito de este trabajo es determinar si ciertos parámetros del sistema de extracción, como el menisco del plasma y la interfaz del haz, pueden modelarse con precisión y, por lo tanto, usarse para predecir con éxito la trayectoria iónica y la forma del haz en un amplio rango. Se analizan varias configuraciones de electrodos en columnas de acelerador y se selecciona una para describirla de manera más detallada en este trabajo.

Palabras clave: Aceleradores lineales, trayectoria iónica, sistemas de extracción, sistemas de aceleración, campos eléctricos, líneas equipotenciales, implantación de iones, imágenes médicas, terapia de protones.

Recepción: Agosto de 2020 / Evaluación: Septiembre de 2020 / Aprobado: Diciembre de 2020

¹ Licenciado en Física. Magister (C) en Ingeniería. Grupo de investigación INSTRUMENTACIÓN CIENTÍFICA & DIDÁCTICA, Universidad Distrital Francisco José de Caldas, ORCID: <https://orcid.org/0000-0002-3208-518X>. Bogotá-Colombia, e-mail: yadiazg@correo.udistrital.edu.co

² Licenciado en Física. Magister en Ciencias-Física. Doctor en Física. Grupo de investigación FISINFOR. Profesor asistente Facultad de Ciencias y Educación, Universidad Distrital Francisco José de Caldas, ORCID: <https://orcid.org/0000-0002-0578-7717>, e-mail: emunevare@udistrital.edu.co

³ Físico. Magister en Ciencias-Física. Doctor en Física. Profesor asistente, Pontificia Universidad Javeriana, Departamento de Física. ORCID: <https://orcid.org/0000-0002-3050-1442>, e-mail: leyvaa@javeriana.edu.co

Víctor Alfonso Díaz Gómez, Edwin Munévar Espitia,
 José Alfonso Leyva Rojas

Introduction

B. J. Holzer (2016) argues that particle accelerators were conceived, designed, and used primarily for research in nuclear physics and high-energy physics... (p. 29). Today, they are increasingly used in fields as diverse as archeology, materials science, biology, and medicine. There are more than 8,000 small low-energy accelerators (up to a few MeV per unit mass for light ions) dedicated to ion implantation, mass spectroscopy, and proton-induced X-ray emission (PIXE). "In the line of surface physics, they focus on the growth and characterization of extremely thin films of materials and the study of their surfaces and interfaces" (Santamaría, 2014, p. 79-80). Accelerator columns are used in industrial applications such as ion implantation, a typical process in materials engineering used to improve the surface properties of materials. "Constant technological advances have made it possible to generate techniques for the surface protection of materials exposed to aggressive media" (Niño, 2011, p. 31). One of the current problems in the high-tech metalworking industry and in the manufacture of precision devices is the development of surface treatment techniques that improve the properties of materials, such as: microhardness, resistance to friction wear, and resistance to corrosion. "Since the 1970s, intensive research has been carried out in the area of surface treatment of building materials by charged particle beams, especially ion beams" (Dulcé, 2016, p. 19). Regarding corrosion, the modification of surfaces includes the application of technologies to obtain the desired properties, leading to the protection of certain types of materials subjected to different aggressive media. "These coatings are potentially suitable for applications intended to protect the surface from wear by abrasion, friction, or chemical action, from cutting tools to prosthetics, so it is important to know their influence on mechanical behavior" (Hermida, 2003, p. 885). From traditional methods, such as enameling or electrodeposition of metals, to more recently developed techniques, such as ion implantation, all are of worldwide interest in mitigating corrosion problems. "Corrosion is mainly a phenomenon that occurs at the surface level, which is why there is a close relationship between the composition of the material and the structure of the films that form on its surface" (Arguello, 2010, p. 17), (Muthukumaran, 2010, p. 2814). "The application of ion implantation technique has shown significant changes in the properties of metals, such as increased resistance to corrosion and increased resistance to fatigue of metals" (k.chu, 1998, p. 3-4). There are several ways to analyze and characterize such structural changes in materials due to ion implantation. This kind of study requires advanced image processing, treatment, and analysis with specialized software. Perez Pereira (2011) argues that, in particular for this task, efficient free software can be found in Java, which provides a safe characterization of these doped materials (p. 107).

On the medical side, an important application of accelerators is diagnostic imaging. "Diagnostic imaging has made an astonishing advance during the 20th century. It is today an essential complementary method of clinical practice. Consequently, it plays a prominent role in therapeutic procedures and medical education" (Esquivel, 2018, p. 225). "One of the main methods of cancer treatment is radiotherapy (RT), where linear accelerators are used. They currently have a volumetric image acquisition system that works through the cone beam computed tomography technique" (Cañas, 2020, p. 1). Physicians and medical students have always needed a good topographical understanding of human anatomy before examining a patient. "In addition, there is also a need for the understanding of cuts sectioned by X-rays, ultrasound, tomography, and resonances, that is, morphological information revealed by new imaging techniques" (Fajardo, 2016, p. 57). The term medical imaging refers to the study of images obtained from the human body and the technology to obtain and process them. Gianfranco Passariello (1995) assures us that from the moment that x-rays were discovered, the hope of being able to see the body inside was born for medicine. This finding is, without a doubt, one of the greatest events in this millennium was the beginning of radiology.. (p.1).

Medical imaging is then intended to provide information to the physician regarding the patient's disease, allowing accurate possible diagnosis. "In recent years, medical teams have improved their ability to generate three-dimensional information." (Escobar, 2009, p. 5). Therefore, software advances in image processing and treatment are required. For example, in the case of cancer, early detection of abnormal cells is of great importance. "It is important to develop a technique for automatic analysis of these images that can support the prognosis of cervical injuries" (Saenz, 2014, p.68). The range of imaging methods in medicine is broad. Among the most used are X-rays, Ultrasound, Computed Tomography (CT), and Magnetic Resonance (MRI). "The usefulness of radiographs for diagnosis is due to the penetration capacity of the rays" (Raudales, 2014, p. 36). X-rays are a type of ionizing electromagnetic radiation that, due to its small wavelength, has the ability to interact with matter. The shorter the wavelength of the rays, the greater their energy and penetrating power. The fundamental components that make up conventional radiological equipment are: the X-ray tube, the radiation generator, and the radiation detector. "The usefulness of radiographs for diagnosis is due to the penetration capacity of the rays. X-rays are fired from the ray tube towards a plate and are attenuated as they pass through the body of the person. This is where absorption and dispersion processes play an important role "(Eastman, 2005, p. 1).

On the other hand, according to the World Health Organization (WHO), cancer is one of the leading causes of death in the world, with 7.7 million deaths (about 13% of all deaths) in 2016, plus 70% of deaths from this cause were registered in low-and middle-income countries. This figure, according to calculations for 2030, will exceed 13.1 million (<http://www.who.int/es/newsroom/factsheets/detail/cancer>). Garza Salazar (2014) argues that treatments for different types of cancer have improved considerably in the last decade as a result of intense basic and applied research together with the development of therapeutic equipment and methodologies... (p. 29). There are 27 proton facilities in the world that take advantage of high-energy physics research accelerators or, more recently, new facilities designed and built for cancer therapy and treatments. "The history of Hadron therapy dates back to 1946, when the American physicist Robert Wilson proposed the use of protons for cancer therapy." (Herranz, 2008, p. 50).

Hadron Therapy has several advantages for treating tumors that require a high degree of precision when they are close to vital organs. "Proton therapy (PT) is the hadron therapy modality (therapy that uses beams of charged particles or ions) that is most popular at the moment in Spain" (Moranchel, 2019, p. 18). This is due to the fact that the hadron beams upon entering the body present less scattering than electron and gamma ray beams. For this reason, healthy tissues and structures close to the beam path receive very little radiation. "Robert Wilson's observations on the potential benefits of proton therapy for cancer treatment created interest among clinical scientists" (Smith, 2009, p. 559). Another clinical option with physical properties similar to proton treatment is that with heavy particles such as carbon ions. In addition, they offer greater biological efficacy in certain types of tumors."The characteristics of radiation constituted by heavy particles make it a very useful tool for therapeutic use. Protons, helium nuclei, and carbon ions are being used successfully in facilities in medical centers around the world "(Lozares, 2008, p. 85). The main goal of this work is to show the importance of computational simulations for the study of the geometry of the field and electric potential for a specific set of electrodes, and their relevance for determining the trajectories of particles immersed in such a field. B. J. Holzer (2016) states that simulations of ion beam extraction can aid in the design of an extraction system and thus characterize the design basis for a column-type ion accelerator... (p. 35). In this work, we will examine the design of an ion accelerator column similar to that shown in Figure 1.

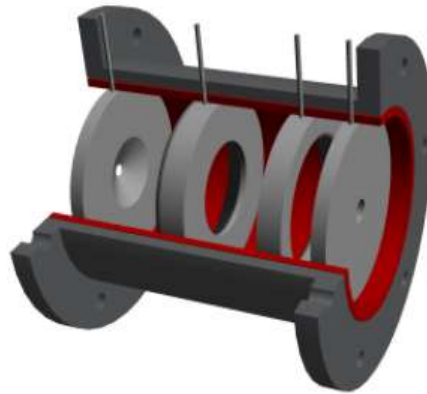


Figure 1. Compact accelerator column designed by LBNL. Source: author.

The data obtained in the current work for the simulated configuration corresponds to the accelerator column modeled in (Leung, 1998, p.225). The calculation software used was IGUN, which in turn was the basis of the research developed in the master's thesis at the Pontificia Universidad Javeriana (Cifuentes, 2019, p.31), which is the starting point of our work.

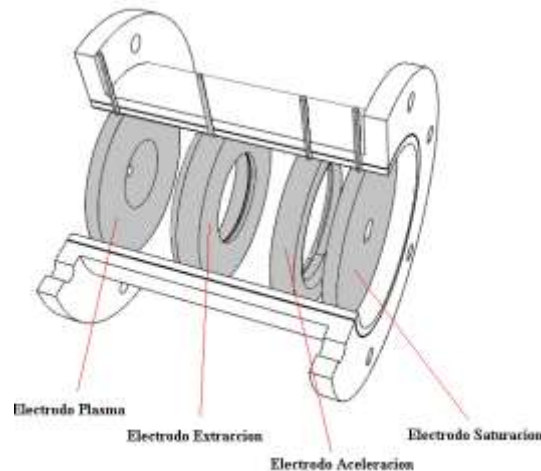


Figure 2. Description of the compact accelerator column designed by LBNL . Source: author.

As illustrated in Figures 1 and 2, the selected accelerator column, drawn in Solid Edge, is composed of four electrodes: plasma, extraction, acceleration, and suppression. A later section will describe the characterization of each of these electrodes.

Computational simulation with JAVA

JAVA is a platform-independent object-oriented programming language with a syntax similar to C++ but simplified. It has great base functionality (increased by the large amount of existing third-party code). For ideal situations in a parallel-plate system, an electric field line simulator written in Java is used to obtain the following figures.

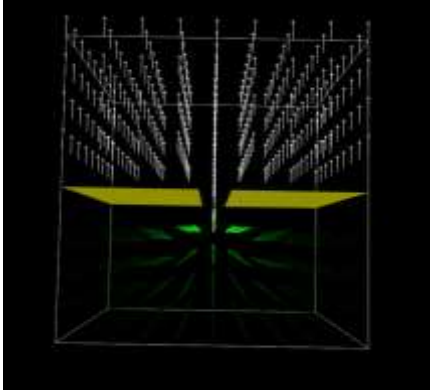


Figure 3. Simulation with JAVA 32, 3D field vectors in a parallel plate system with a slotted plate. Source: reference. (Electricity and magnetism: Static (s.f.). Electrostatic fields applet 2D- 3D. Recovered from <https://www.falstad.com/vector2de>, <https://www.falstad.com/vector3de>).

As illustrated in Figure 3, the electric field vectors in white are organized and all point in the same direction in the area between the parallel plates. The vectors in green represent the movement of the ions within the plasma source when the plates are connected to the high-voltage source. This JAVA simulation code allows us to vary the force field between the plates, as well as vary the number of particles and the width of the groove in the plasma electrode plate.

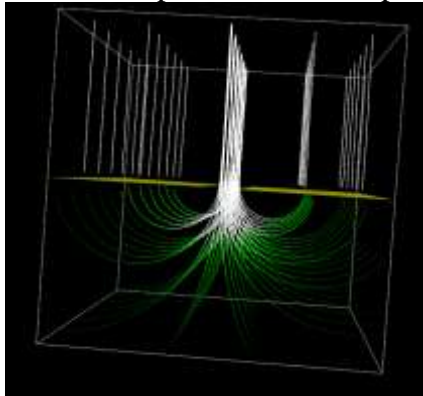


Figure 4. Simulation with JAVA 32, 3D flow lines in a parallel plate system with a slotted plate. Source: reference. (Electricity and magnetism: Static (s.f.). Electrostatic fields applet 2D- 3D. Recovered from <https://www.falstad.com/vector2de>, <https://www.falstad.com/vector3de>).

With an electric field applied, a fixed number of particles and a diameter of 5 mm were used for the width of the slot, yielding the field vectors and three-dimensional field lines within the column (see Figure 4). An important characteristic of equipotential lines is that they are perpendicular to the electric field lines at all points (see Figure 5), which results from the properties of the gradient operator. The electrode (blue color) is located in the nozzle of the ion source. In the simulation, it is observed how the vectors of the electric field are organized within the system of parallel plates.

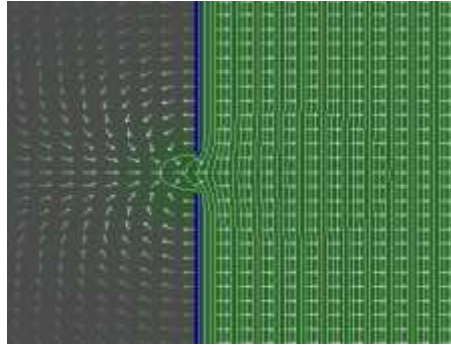


Figure 5. Equipotential lines and field vectors. Source: reference. (Electricity and magnetism: Static (s.f.). Electrostatic fields applet 2D- 3D. Recovered from <https://www.falstad.com/vector2de>, <https://www.falstad.com/vector3de>).

Figure 6 shows the electric field lines in the accelerator column. A charged particle that is in a region where there is an electric field experiences a force equal to the product of its charge and the intensity of the electric field. If the field is uniform, the force is constant and so is the acceleration.

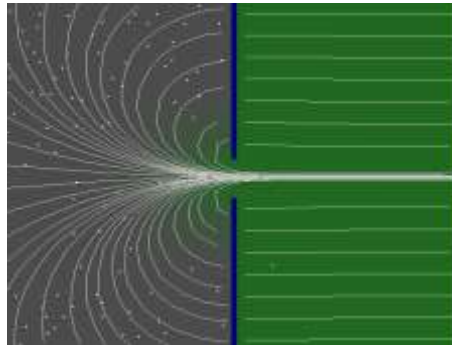


Figure 6. Simulation with JAVA 32, ion trajectory in a parallel plate system with a slotted plate. Source: reference. (Electricity and magnetism: Static (s.f.). Electrostatic fields applet 2D- 3D. Recovered from <https://www.falstad.com/vector2de>, <https://www.falstad.com/vector3de>).

As we can see in Figure 7, the simulation shows that the diameter of the groove in the electrode that connects to the ion source directly influences the trajectory and focus of the particles. In the image, four simulations are detailed where the width of the slot is varied.

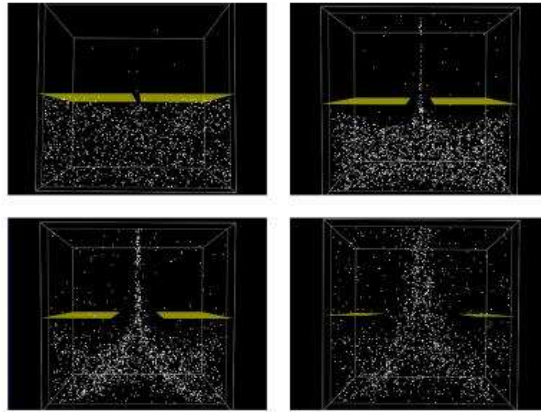


Figure 7. Simulation of ion trajectories in a parallel-plate system with a slotted plate and different separation distances. Source: reference (Electricity and magnetism: Static (s.f.). Electrostatic fields applet 2D- 3D. Recovered from <https://www.falstad.com/vector2de>, <https://www.falstad.com/vector3de>).

If the groove of the electrode is too small, the particles have no possibility of entering the extraction zone; if it is too large, many particles can not be focused in the ion beam. Thus, with the help of java, we can have a visualization of the trajectory of the particles within two plates connected to a potential difference and with one of the grooved plates.

II. Materials and methods

Electrode construction

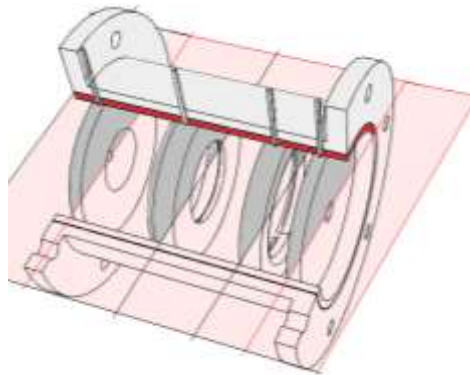


Figure 8. Cross section of the accelerator column. Source: author.

In order to facilitate the experimental study and the development of data collection, a cross section of the column is made in such a way that a 2D view of the electrodes and the acceleration system is obtained (see Figure 8). From the cross section of the column, a 2D image of the electrodes is obtained in blue (Figures 9, 10, 11, 12). Thus, we can observe a top view of the electrodes.



Figure 9. Cross section of the plasma electrode (top view). Source: author.

In this way, we have a graphical representation of each of the electrodes in 2D to proceed to draw them and move on to the construction phase.

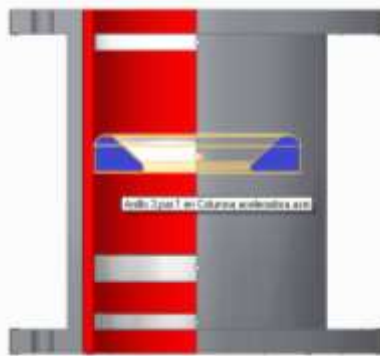


Figure 10. Cross section of the extraction electrode (top view). Source: author.

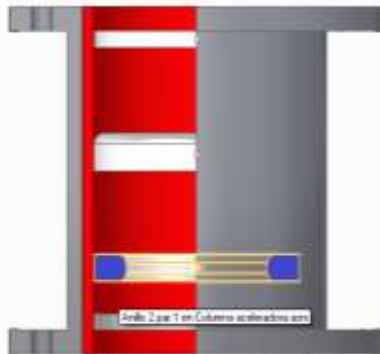


Figure 11. Cross section of the acceleration electrode (top view). Source: author.



Figure 12. Cross section of the saturation electrode (top view). Source: author.

Finally, we obtain a two-dimensional image of the accelerator column (see Figure 13), which shows a top view of a section of the column. We then proceed to draw and construct the column's corresponding components using this graphical representation.

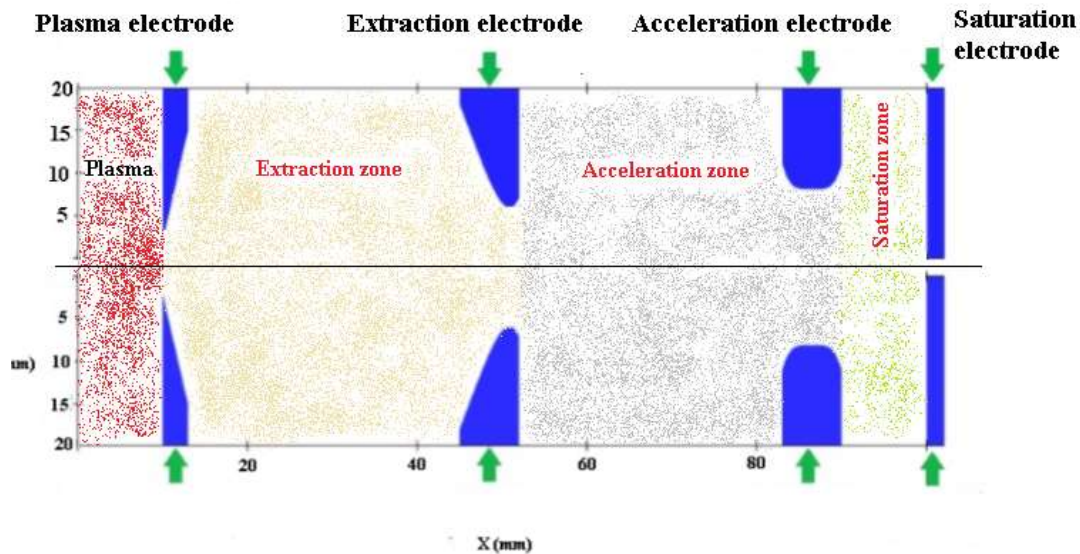


Figure 13. Top view of a cross section of the accelerator column (Leung K. N, 1998)
(Cifuentes J. A. 2019)

The column is made up of 4 electrodes separated from each other at a certain distance, which generates 3 specific areas where the particles are accelerated (see Figure 13). The plasma electrode is located at the output of the RF source, with a 2.5 mm radius and a wedge-shaped geometry, initially flat and ending in a point. The extraction electrode is located at a distance of 32 mm from the plasma electrode, has a semi-triangular geometry, and its tip ends in a semicircle. The region between this pair of electrodes is known as the extraction zone and its geometry differs from a pair of flat-parallel plates.

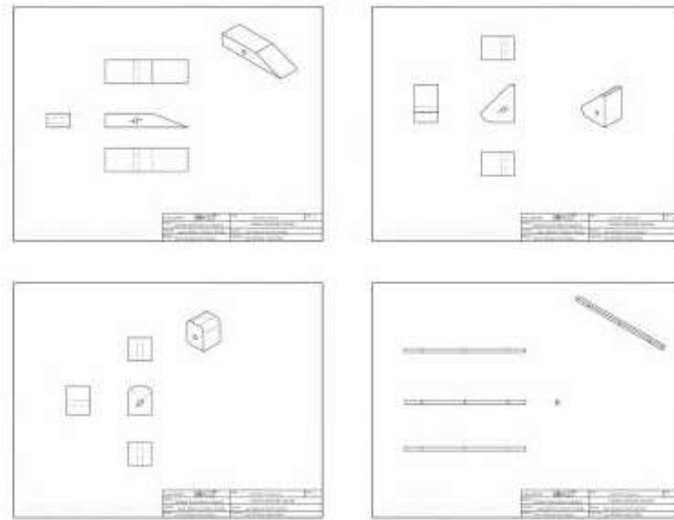


Figure 14. Drawing of the electrode planes made with Solid Edge 2020 f. Source: author.

The acceleration electrode is located at a distance of 31 mm from the extraction electrode. Its geometry is initially rectangular and ends in a semicircle with a radius of 0.5 cm. Finally, there is a suppression electrode that is located 12 mm from the accelerator electrode. From the electrodes cross section of the column and the planes drawn in Solid Edge, the design of each of them is obtained. Figures 14 and 15 show the drawing of the planes and the design of the electrodes selected and designed in Solid Edge. The electrodes were made of aluminum according to the selected scale.

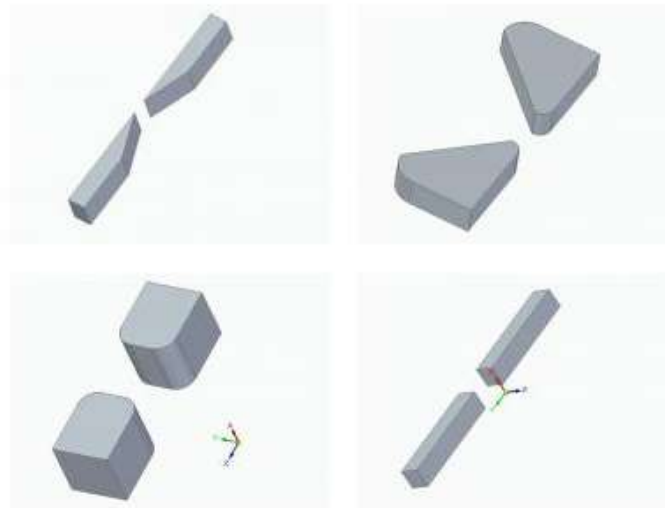


Figure 15. Design in Solid Edge 2020 f of the accelerator column electrodes. Source: author.

Finally, as with the pair of constructed electrodes that will simulate the extraction electrode (Figure 16), we proceed with the construction of the remaining electrodes⁴ that make up the selected column (Figures 17, 18, and 19). When building and machining parts on CNC lathes or conventional lathes, great care needs to be taken due to the precision of the needed parts. There are different methods and types of tools for this task. For our future electrodes, we would like to implement an artificial vision system. (Forero, 2013, p. 36).



Figure 16. A pair of electrodes made of aluminum that simulate the extraction electrode.
Source: author.



Figure 17. A pair of electrodes made of aluminum that simulate the plasma electrode.
Source: author.



⁴ All the electrodes were built in the company AXIOMÁTICA ST. This is a Colombian company located in Bogotá D.C that provides mechanical and electrical engineering services. They design and calculate systems in the fields of mechanisms and machines with everything regarding heat exchange structures, control and power electrical installations.

Figure 18. A pair of electrodes made of aluminum that simulate the acceleration electrode.
Source: author.



Figure 19. Electrode made of aluminum that simulates the saturation electrode. Source: author.

III. Experimental Measurements

Electrolytic tray

To describe the trajectories of the ions, it is necessary to find both the electric field vectors and the field lines within the system. To accomplish this, it is critical to determine the potential distribution in each region of the electrolytic tray. The accelerator column geometries need to be schematized in one plane, which requires a cross section. This means that each electrode in the column will be represented by two flat electrodes connected to each other and with a previously selected characteristic geometry. In order to reduce the positional uncertainty, a matrix of 6000 holes spaced 2 mm apart on both axes was constructed on an acetate sheet as shown in Figure 20. This means that a total of 6000 potential data points were measured on the tray designed for this experiment. Manual precision is required to achieve a match between the points on the millimeter sheet and the gaps on the acetate sheet.

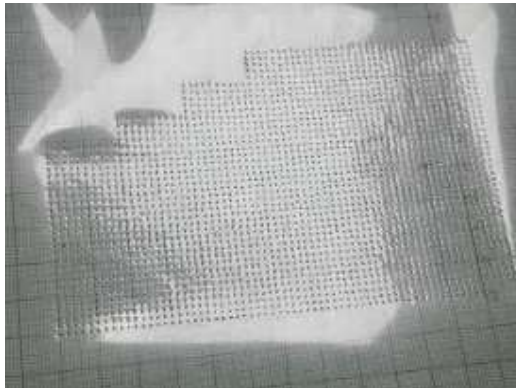


Figure 20. Dot matrix composed of 6000 holes. Image taken against the light to appreciate the distribution of the holes. Source: author.

The potential distribution in each region is obtained from the equipotential lines, which are determined by schematizing the geometries of the column in a plane. As a result, each electrode of the column will be represented by two flat aluminum electrodes, connected to each other and with a characteristic geometry. To carry out the experiment, the pairs of electrodes were built in larger dimensions but keeping the proportions of the original model. The experimental method used was

based on the construction of the different parts of the electrodes that geometrically model the parts of the acceleration column in 2D (Figure 21).

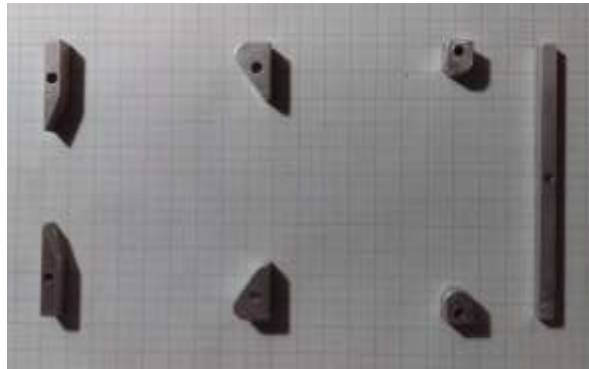


Figure 21. Location of the electrodes on the acetate sheet with 6000 points. Source: author.

The electrodes were fixed with special glue on the acetate sheet and the whole system was introduced into a glass tray.

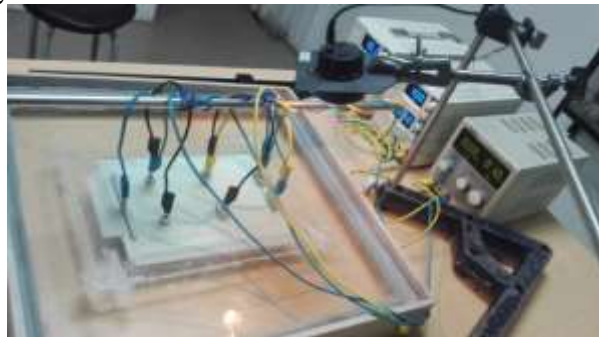


Figure 22. Experimental setup at the Physics Laboratories of the Universidad Distrital Francisco José de Caldas - Macarena A. Source: author

Each of the electrodes is subjected to a voltage which is related to the plasma electrode. The selected values were: 100 kV for extraction, 200 kV for acceleration, and 190 kV for suppression. Thus, for the development of experimental practice and data collection, a circuit representing a diminished scale of our acceleration system was generated. Three voltage sources simulate the three regions of the accelerator column (see Figure 22). The voltage between the plasma electrode and each point of the matrix was measured. Each point requires waiting time (approximately 10 s) to achieve relative stability in the measurement. A matrix $V(x, y)$ was obtained (see Figure 23), which establishes the different potential values along the column. The data matrix obtained was plotted in MATLAB R2020a.

The entire data set for this study was collected at the Physics Laboratory (Macarena A) of the Universidad Distrital Francisco José de Caldas.

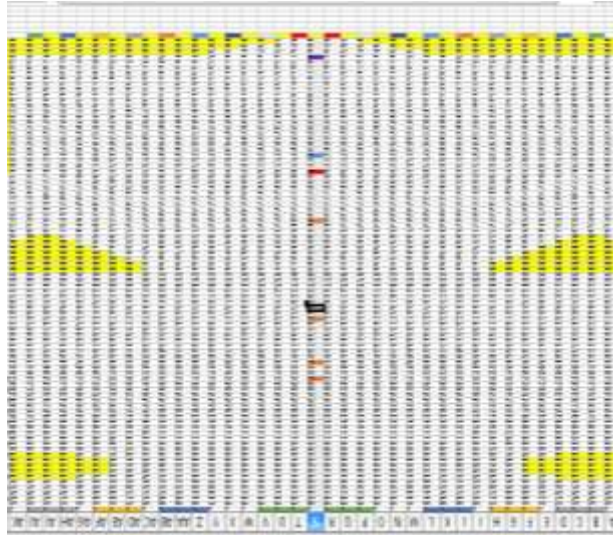


Figure 23. Matrix $V(x, y)$ that establishes the different potential values along the column. 6000 data points were taken. Source: author.

IV. Results and discussions

Computational Simulation with MATLAB R2020a

MATLAB (short for MATrix LABORatory) is a numerical computing system that offers an integrated development environment (IDE) with its own programming language (M language). Its basic features include the manipulation of arrays, the representation of data and functions, the implementation of algorithms, the creation of user interfaces (GUI) and communication with programs in other languages. MATLAB combines a streamlined desktop environment for iterative analysis and design processes with a programming language that expresses matrix mathematics. The matrix of data obtained experimentally in the laboratory is used to generate different types of graphs with the MATLAB R2020a tool package. The data matrix is used to obtain the equipotential lines, field vectors, and electric field lines to finally describe the trajectories of the ions within the electrolytic tray. The vector field is determined from $\mathbf{E} = -\nabla V$ by using a central difference numerical method. The data measured in the electrolytic tray is processed and the vector field represented in Figure 24 is obtained.

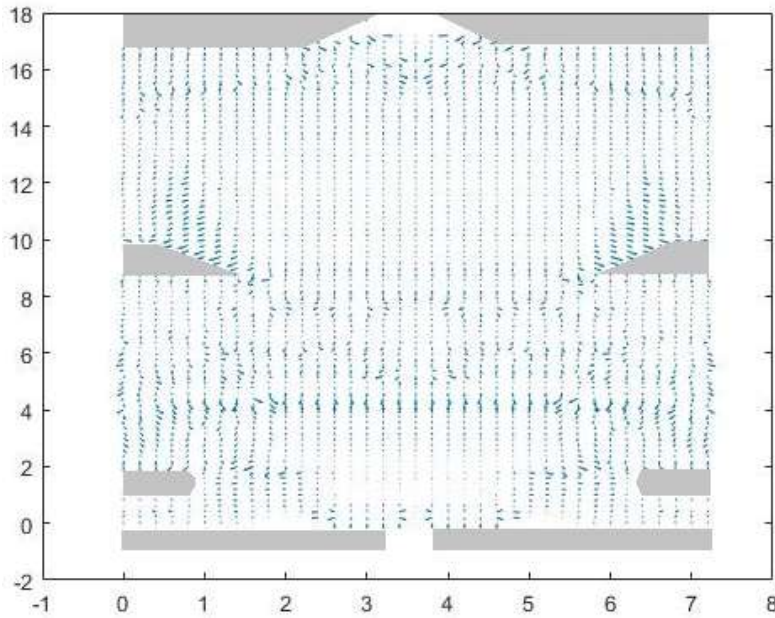


Figure 24. Vector field obtained for the accelerator column. Source: author.

Equipotential lines are the contour lines that trace and pass through points having the same electric potential. As can be seen in Figure 25, the equipotential lines are always perpendicular to the electric field vectors.

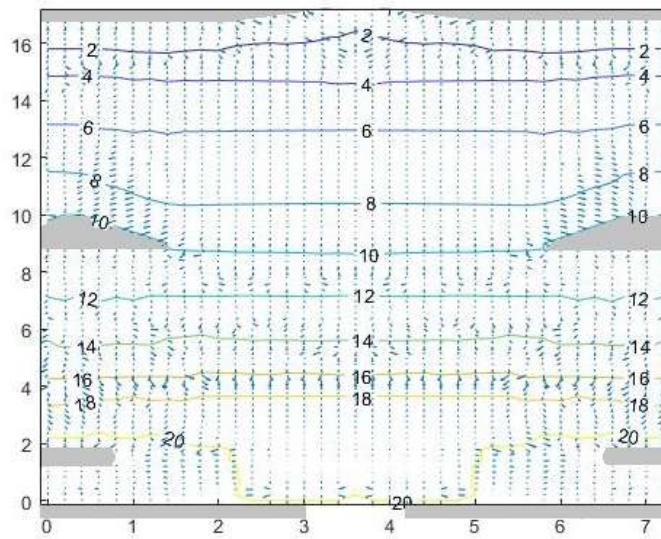


Figure 25. Equipotential lines and field vectors obtained for the accelerator column. Source: author.

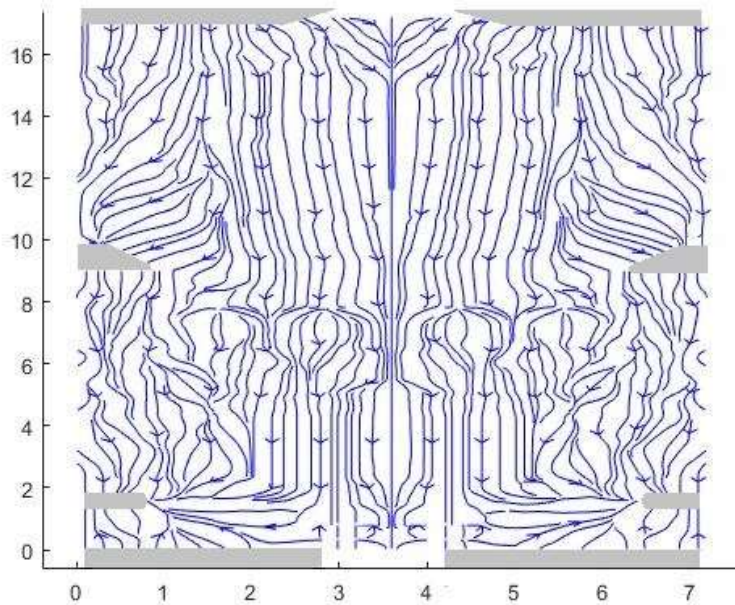


Figure 26. Electric field lines generated within the accelerator column. Source: author.

Figure 26 shows the field lines within the accelerator column. Selected and constructed electrodes are shown in gray color.

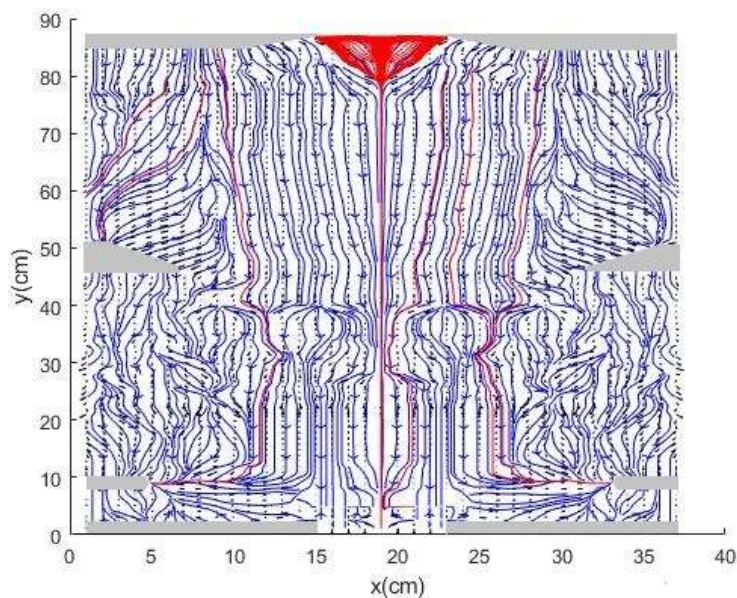


Figure 27. Ion trajectories and field lines generated within the “unfocused” accelerator column. Source: author.

Figure 27 allows us to visualize in detail the trajectories of some particles that cannot be focused and therefore do not enter the ionic beam. It is clearly observed that the “unfocused” particles are directed along the electric field lines towards the closer electrodes. In this case, the majority goes to the saturation electrode.

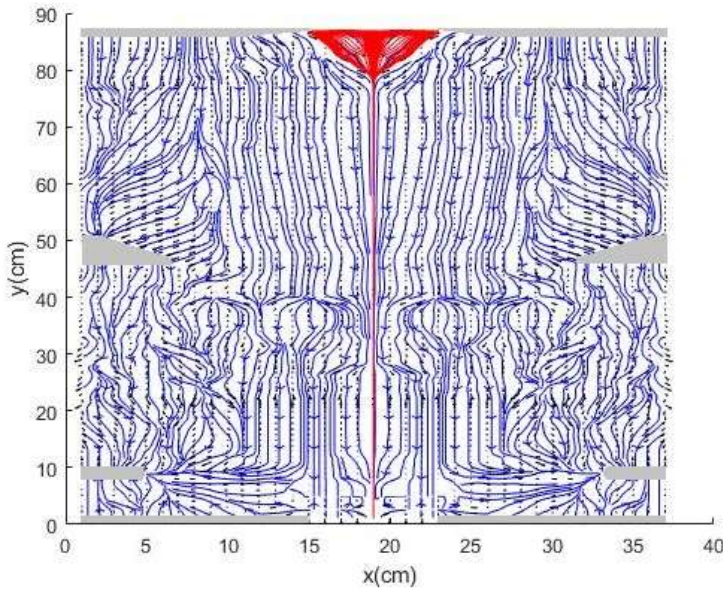


Figure 28. Ion trajectories and field lines generated within the focused accelerator column.

Source: author.

It is important to know the covering range of the ions so that they can be effectively focused and pinpoint where on the electrolytic tray they fall out of the line of action. Figure 28 shows the focused trajectories of the accelerated ions in the entire column. As can be seen, there are seven electrodes proposed in our hypothesis and around each the equipotential lines are represented and, perpendicular to these, the electric field vectors \mathbf{E} .

Description of the motion of protons in the accelerator column

In general, a particle of mass m and charge q , initially placed at rest in a uniform electric field \mathbf{E} and then released, describes a motion that resembles that of a body falling in the Earth's gravitational field. The uniform acceleration is given by:

$$\vec{a} = \frac{\vec{E} q}{m} \quad (1)$$

The trajectory, velocity, and kinetic energy of charged particles as a function of the electric field correspond to [22]:

$$\vec{r} = \frac{\vec{E} q}{2m} t^2 \quad (4)$$

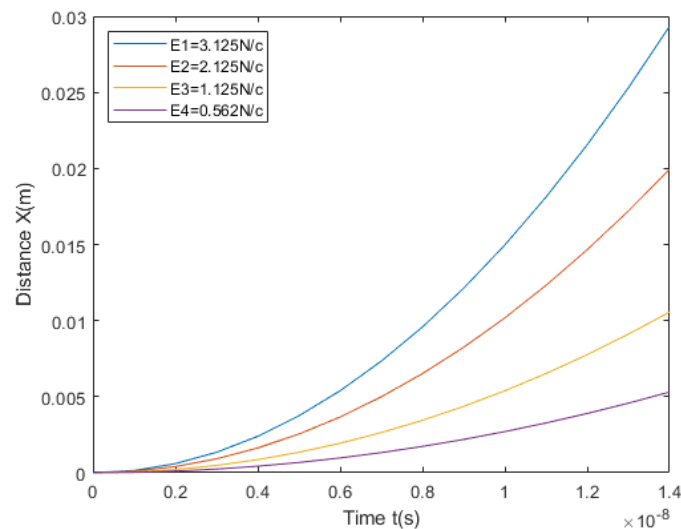
$$\vec{v} = \vec{v}_0 + \frac{\vec{E} q}{m} t \quad (5)$$

$$K = \frac{1}{2} m |\vec{v}|^2 \quad (6)$$

In total, there are three areas in the column where the particles are intercepted by the field: the extraction zone, the acceleration zone, and the saturation zone. In these areas, the particles vary their speed due to the electric field generated between the electrodes. The traveling distance, velocity, acceleration, and kinetic energy of the particles in the first area, or the so-called extraction zone, are described in this article. It has to be taken into account that in this case, the system is

assumed to behave like a system of parallel plates. That is to say, the electric field vector is taken as approximately uniform in the extraction zone. When observing Graph 1, one can say that the greater the electric field E applied to the protons at a given time, the greater the distance traveled. With an electric field of $E_1 = 3.125 \frac{N}{c}$, they travel a distance of 32 mm in a time of 14.629 ns. The varying slope of the graph indicates that the speed is increasing.

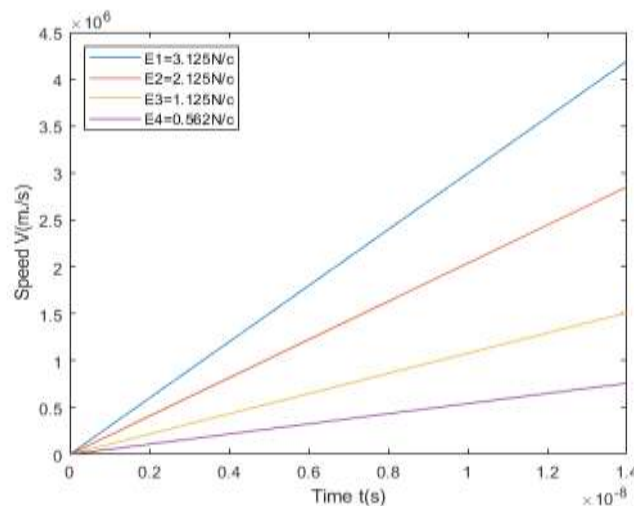
Distance vs time with different E fields



Graph 1. Distance vs time in the extraction zone with a distance of 32 mm between the first two electrodes and four different field intensities. Source: author.

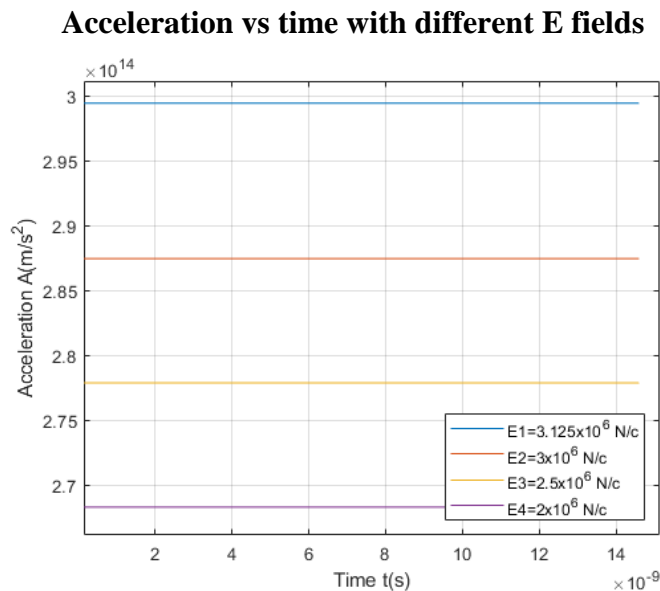
Taking into account that the proton in the slot of the plasma electrode is initially at rest, we use the laws of non-relativistic kinematics and obtain Graph 2. It is observed that the greater the electric field used between the electrodes is, the higher the speed of the protons is when passing through the extraction zone.

Speed vs time with different E fields

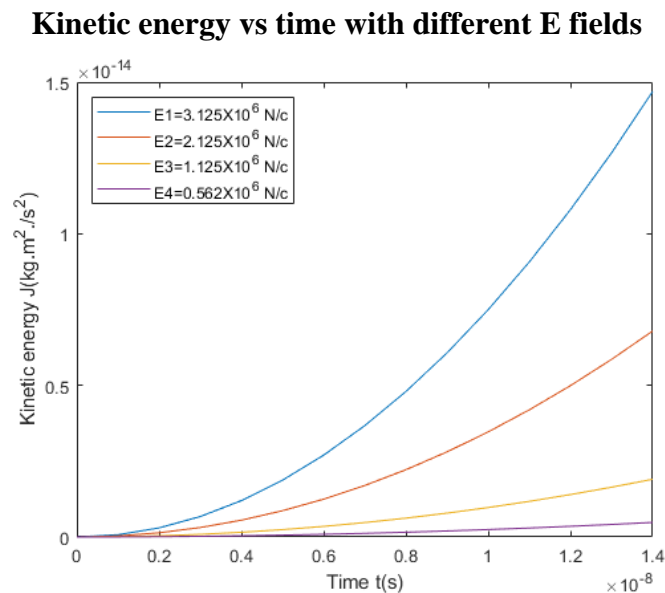


Graph 2. Speed vs time in the extraction zone with four different field intensities. Source: author.

The acceleration vs. time relation for protons moving in the extraction zone of the column is shown in Graph 3. As expected, the acceleration remains constant over time.



Graph 3. Acceleration vs time in the extraction zone with four different field intensities. Source: author.



Graph 4. Kinetic energy vs time in the extraction zone. Source: author.

The speed acquired by protons in the column is directly proportional to the electric field generated by the electrodes as they are connected to a source with 100 kV between the plasma electrode and the extraction electrode. Note that with an electric field of $E = 3.125 \times 10^6 \frac{N}{c}$, the particles acquire a kinetic energy of $E_k = 1.6020 \times 10^{-14}$ Joules. If the field decreases, the kinetic

energy decreases as well; a small change in the value of the electric field leads to a large change in the velocity of the protons.

Results obtained for protons located inside the accelerating column

Table I shows a summary of all the values obtained for a proton in the extraction zone with the conditions given in our selected accelerator column.

Extraction zone	
Electric field	$E_{\blacksquare} = 3.1250 \times 10^6 \frac{N}{C}$
Traveling distance	$x_{\blacksquare} = 32 \text{ mm}$
Initial velocity	$V_o = 0 \frac{m}{s}$
Final velocity	$V_f = 4.3775 \times 10^6 \frac{m}{s}$
Acceleration	$a_{\blacksquare} = 2.9942 \times 10^{14} \frac{m}{s^2}$
Kinetic energy	$K_{\blacksquare} = 1.6020 \times 10^{-14} \text{ Julios}$
Proton mass	$m_p = 1.672 \times 10^{-27} \text{ kg}$
Time of flight	$t = 14.629 \times 10^{-9} \text{ s}$
Voltage applied between electrodes	$u = 100 \text{ kV}$

Table 1. Found data of accelerated protons in the extraction zone within the selected accelerator column

Comparison of the MATLAB R2020a simulation with the Ibsimu and IGUN programs

A comparison with the simulations developed in this work and in Verbeke J. M. (2000) and Cifuentes J. A. (2019) is presented in this section. The comparison focuses on the results obtained for the extraction zone, in particular for the analysis of menisci and trajectories using normal conditions typical of a radio frequency source.

Simulation Ib Simu

Figure 29 shows the Ib Simu simulation of the particle trajectories in the extraction zone for a potential of -100 kV with a separation distance of 45 mm between the plasma and extraction electrodes (Cifuentes, 2019, p. 56).

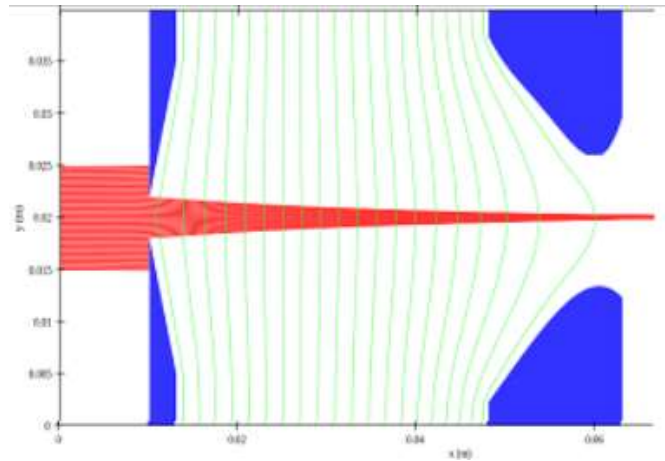


Figure 29. Simulation obtained in the Master's thesis “Preliminary Evaluation of D Acceleration in a Compact High Flow D-D Neutron Generator” (Cifuentes, 2019).

IGUN simulation

Figure 30 shows the IGUN simulation of the particle trajectories in the extraction zone for a potential of -120 kV with a separation distance of 42 mm between the plasma and extraction electrodes. Out of the different simulations presented in (Verbeke, 2000, p. 148), only this one is shown because of its similarity to the potential studied in this work.

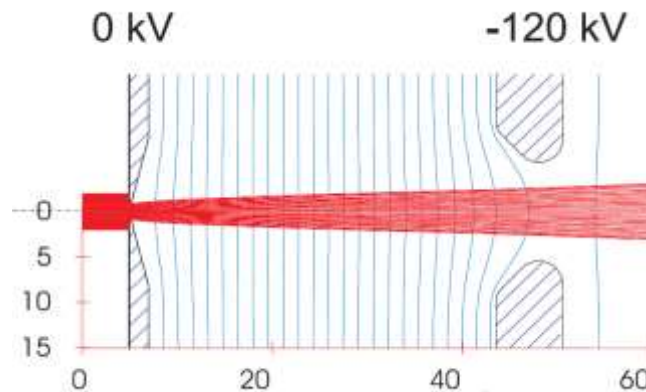


Figure 30. Simulation obtained in the PhD thesis “Development of High-Intensity D-D and D-T Neutron Sources and Neutron Filters for Medical and Industrial Applications” (Verbeke, 2000).

MATLAB R2020a simulation

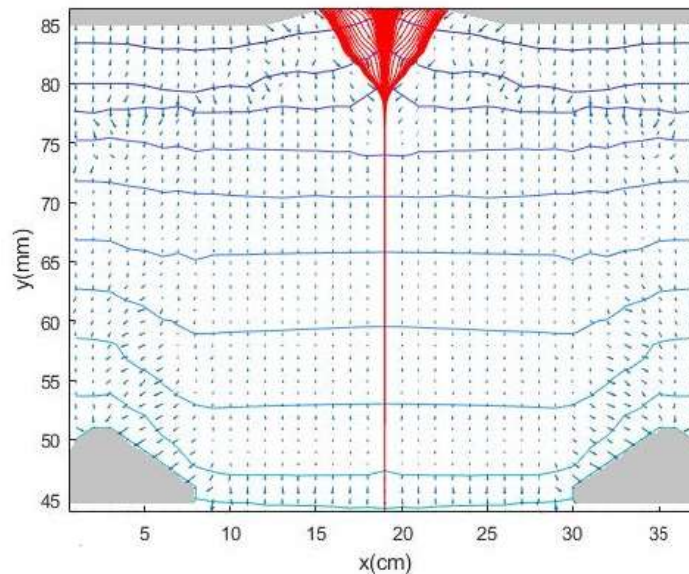


Figure 31. Simulation obtained in this work as part of the ongoing Master's thesis "Preliminary design of a prototype for a light ion accelerator". Source: author.

The simulation developed in this work with MATLAB R2020a can be seen in Figure 31. It shows the simulation of the trajectories of the protons in the extraction zone for a voltage of -100 kV with a separation distance of 32 mm between the plasma electrode and the extraction electrode. This is the simulation obtained from the data taken in the Physics Laboratory of the Universidad Distrital (Macarena A) with the electrolytic tray and the electrodes duly selected and constructed. A comparison of Figures 29, 30, and 31 reveals clearly that the equipotential lines generated in the three cases within the accelerator column are very similar; these generated lines surround and take the contour shape of the corresponding electrodes. It is observed that the field vectors are perpendicular to these lines, leading to changes in the trajectories of the treated particles. Finally, it can be seen that in the three simulations, it is possible to focus the particles in such a way that a particle beam is generated with a stable direction.

Conclusions

The linear accelerator column studied in this work consists of three regions with increasing ion velocity: the extraction zone, the acceleration zone, and the saturation zone. The column is composed of four electrodes: plasma, extraction, acceleration, and saturation. The system can extract protons, carbon ions, and helium ions, depending on the electric field setting and the geometry of the electrodes. The geometries of the selected electrodes were simulated on a larger scale $\times 10$. The parameters examined: the applied voltage and the separation distance, were varied to study their effect on the structure of the ion accelerator column. The potentials used in the measurement phase (from 1 to 20 volts) as well as the distances between electrodes are similar to those proposed in the LBNL article Verbeke J. M. (2000).

An electrolytic tray and a set of electrodes were designed and built for data collection and code validation with MATLAB R2020 a, as a method to simulate the trajectories of the ions in the electrolytic tray. Such a validation took place in two parts: first, by comparing it with the

accelerating column proposed in Cifuentes J. A. (2019); and second, through an experimental procedure and data collection. MATLAB was then used to observe the behavior of the ion beam by varying the extraction kilovoltage and the distance between the plasma electrode and the extraction electrode. Thus, in the simulation, it was observed that the beam focusing decreased as the separation distance between the first two electrodes increased. Each separation distance and applied voltage has an optimal beam extraction condition.

The simulation of the ion trajectories in the column allowed us to determine the region where the field lines generated in the system extend beyond the line of action of the particles and can not focus them. Ion trajectory calculation shows a stable beam distribution and improved beam quality by having a suitable diameter at the ion source nozzle.

Bibliographic references

- Arguello A., and Sanchez J. C. (2010). Experimental evaluation of the implantation of Ti and N ions in the resistance to corrosion in carbon steel AISI SAE 1010. Universidad industrial de Santander, Graduate project, Faculty of Physicochemical Engineering. Bucaramanga.
- Cañas D. L. (2020). Study of the viability of CBCT images for treatment planning (Master Thesis). Ponticia Universidad Javeriana, Faculty of Sciences, Department of Physics, Bogotá D.C, Colombia.
- Cifuentes J. A. (2019). Preliminary Evaluation of D Acceleration in a Compact High Flow D-D Neutron Generator (Master Thesis). Ponticia Universidad Javeriana, Faculty of Sciences, Department of Physics, Bogotá D.C, Colombia.
- Chu P. K., and Cheung N. W. (1998). Microcavity engineering by plasma immersion ion implantation, *Materials Chemistry and Physics*. Volume 57, Number 1, Pages 1-16.
- Eastman G. W., Wald C., and Crossin J. (2005). Getting started in clinical radiology, from image to diagnosis. Germany.
- EducationalApplets:<https://www.falstad.com/vector2de>,<https://www.falstad.com/vector3de>.
- Escobar A., and Calderón, L. A. (2009). THREE-DIMENSIONAL LOWER LIMB MODEL BASED ON MAGNETIC RESONANCE IMAGES. Universidad Distrital Francisco José de Caldas. *Revista Visión Electrónica* Vol. 3 No. 1.
- Esquivel L., García Y. F., and González Y. J. (2018). A look at the means for diagnostic imaging from medical education. 10 (1): ISSN 2077-2874 RNPS 2234 Santa Clara Jan.-Mar. EDUMECENTRO.
- Fajardo M. (2016). The scientific-technical revolution and its impact on the medical sciences. M. Hernández Pino. Havana: Virtual University of Health.
- Forero J., Bohórquez C., and Ruiz V. H. (2013). AUTOMATED MEASUREMENT OF TURNED PARTS USING ARTIFICIAL VISION. *Revista Visión Electrónica* Year 7 No. 2 pp. 36 - 4.
- Garza J. G., and Juárez P. (2014). *Cáncer*. Autonomous University of Nuevo León. Centro, Monterrey, Nuevo León, México, C.P. 64000 First edition, 2014. ISBN: 978-607-27-0215-8
- Hermida E. B. (2003). Influence of ionic implantation on film traction from al 8006. SAM 2000 Conference - IV Latin American Colloquium on Fracture and Fatigue, August 2000, 885-891. Buenos Aires.
- Herranz J. L., Herraiz E., Vicente S., España J., Cal-Gonzalez J. L., and Udías J. M. (2008). Hadrontherapy. First Complutense Meeting for the Dissemination of Nuclear and Particle Physics.

- Holzer B. J. (2016). Introduction to Particle Accelerators and their Limitations. Published by CERN in the Proceedings of the CAS-CERN Accelerator School: Plasma Wake Acceleration, Geneva, Switzerland, edited by B. Holzer.
- Leung K. N., Lee Y., Verbeke J. M., Vujic J., Williams M. D., Wu L. K., and Zahir N. (1998). A Sealed-Accelerator-Tube Neutron Generator for Boron Neutron Capture Therapy Application (Ph. D. Thesis). Lawrence Berkeley National Laboratory University of California Berkeley USA. CA 94720. Nuclear Engineering Department. La Jolla, CA.
- Lozares S., Mañeru F., and Pellejero S. (2009). Heavy particle radiation therapy. Radiophysics and Radiological Protection Service. Navarra Hospital. Pamplona. An. Sist. Sanit. Navar. Vol. 32, Suplemento 2.
- Moreno H. J., Dougar-Jabon V. D., and Tsygankov P. A. (2016). ION IMPLANTATION. Universidad Francisco de Paula Santander, A.A. 1055 Cúcuta, Colombia, Universidad Industrial de Santander, A.A. 678 Bucaramanga, Colombia, Moscow Bauman State Technical University, Moscow, Russia.
- Moranchel I. L., Mand aurelos P. I. (2019). Proton Therapy: state of the art and clinical applications. Revista oficial de la sociedad española de enfermería oncológica. ENFERM ONCOL VOL.21. N.2.
- Muthukumar V., Selladurai V., Nandhakumar S., and Senthilkumar M. (2010). Experimental investigation on corrosion and hardness of ion implanted AISI 316L stainless steel. Materials & design technology. Department of Mechanical Engineering, Kumaraguru College of Technology, India, Volume 31, pages 2813-2817.
- Niño E. D. (2011). Surface modification of an AISI SAE 1045 steel through the implantation of nitrogen and titanium ions. ITECKNE Vol. 8 Número 1 • ISSN 1692 - 1798
- Passariello G, and Mora F. (1995). Medical Images: acquisition, analysis, processing and interpretation. Universidad Simón Bolívar. Equinox, Editions of the Simón Bolívar University; printed in venezuela 1ra. edicion.
- Perez M. R., Hernández H. A., and Güiza G. N. (2011). Application for processing metallographic images from PME3. Universidad Distrital Francisco José de Caldas, Bogotá D. C., Colombia. Revista Visión Electrónica Vol. 5 No. 2.
- Raudales I. R. (2014). DIAGNOSTIC IMAGES: CONCEPTS AND GENERALITIES Rev. Fac. Cienc. Med.
- Santamaría R. A. (2014). Feasibility study for the construction and operation of a particle accelerator in Spain. Superior technical school of engineering (ICAI), Madrid.
- Saenz J. G., Camargo L. H., and Camargo E. (2014). Color descriptors for cytology smear images analysis. Research Group Engineering and Nanotechnology for Life (INVID). Universidad Distrital Francisco José de Caldas, Bogotá D. C. DIGITI Research Group, Universidad Distrital Francisco José de Caldas, Bogotá D. C. Vol. 8 No. 2 July-December, Bogotá (Colombia).
- Smith A. R. (2019). Proton Therapy. Department of Radiation Oncology, The University of Texas M. D. Anderson Cancer Center, 1515 Holcombe Boulevard, Houston, Texas 77030 Med Phys. 2009 Jan 26 [Accessed 2019 Apr 20]; 36 (2): 556-68.
- Verbeke J. M. (2000). Development of High-Intensity D-D and D-T Neutron Sources and Neutron Filters for Medical and Industrial Applications (Ph. D. Thesis). Engineering - Nuclear Engineering. University of California, Berkeley

World Health Organization, February 1, (2018). [Online]. Available:
<http://www.who.int/es/newsroom/fact-sheets/detail/cancer>.